Author/s:
Kameneva, T;Zarelli, D;Nesic, D;Grayden, DB;Burkitt, AN;Meffin, H

Title:
A comparison of open-loop and closed-loop stimulation strategies to control excitation of retinal ganglion cells

Date:
2014-11-01

Citation:
Kameneva, T., Zarelli, D., Nesic, D., Grayden, D. B., Burkitt, A. N. & Meffin, H. (2014). A comparison of open-loop and closed-loop stimulation strategies to control excitation of retinal ganglion cells. Biomedical Signal Processing and Control, 14 (1), pp.164-174. https://doi.org/10.1016/j.bspc.2014.07.015.

Persistent Link:
https://hdl.handle.net/11343/299575

A comparison of open-loop and closed-loop stimulation strategies to control excitation of retinal ganglion cells

Tatiana Kameneva[1,2,⋆,#], Daniele Zarelli[1,2,⋆], Dragan Nešić[2], David B. Grayden[1,2,3,4], Anthony N. Burkitt[1,2,3,4], Hamish Meffin[4,1,2] *

Abstract

Currently, open-loop stimulation strategies are prevalent in medical bionic devices. These strategies involve setting electrical stimulation that does not change in response to neural activity. We investigate through simulation the advantages of using a closed-loop strategy that sets stimulation level based on continuous measurement of the level of neural activity. We propose a model-based controller design to control activation of retinal neurons. To deal with the lack of controllability and observability of the whole system, we use Kalman decomposition and control only the controllable and observable part. We show that the closed-loop controller performs better than the open-loop controller when perturbations are introduced into the system. We envisage that our work will give rise to more investigations of the closed-loop techniques in basic neuroscience research and in clinical applications of medical bionics.

1 Introduction

Most currently used stimulation strategies for medical bionic devices rely upon open-loop control of the stimulation levels. The open-loop strategies may involve the machine-learning of the algorithm parameters or changing the algorithm parameters based on the patient's performance (slow-time scale); however, these strategies do not change stimulation parameters on a pulse-by-pulse basis in response to the evoked activity (fast-time scale), i.e. the level of stimulation does not change in response to any continuous measurement of the level of neural activity that is generated.

While many stimulation strategy algorithms in bionic devices have been successful using open-loop techniques [8], [16], [35], the outcomes differ from patient to patient [1], [12], [38], [48], [59]. For example, the benefits of the cochlear implant may vary even among patients with similar otologic pathologies and with the same type of the cochlear implant system [48].

** contributed equally, [1]NeuroEngineering Laboratory, The University of Melbourne, Australia. [2]Department of Electrical and Electronic Engineering, The University of Melbourne, Australia. [3]Bionics Institute, Australia. [4]National ICT Australia, Victoria Research Laboratory, Australia. #corresponding author: tkam@unimelb.edu.au.

It has been shown that a customized controller in a bionic device allows the manipulation of specific patient-based neural responses [2], [50]. By monitoring neural response and adjusting stimulation parameters using closed-loop control techniques, it is possible to optimize the stimulation on-line based on the acquired data. More effective stimuli are delivered by utilising neuronal recording in a feedback loop to control neurostimulation on a continuous basis. At present, to fit stimulation parameters requires repeated patient's visits to a clinic. This is a major commercial impediment and the parameter's optimization is done in a sub-optimal way. Closed-loop techniques may minimize the time to fit stimulation parameters while in a clinic. Additional benefits of using feedback in neuroprosthetic stimulation may include selective and controlled effects on populations of neurons, directing the electric current based on the response of the targeted neural elements, and reduction in power consumption, since a stimulator is activated only when required, delivering the precisely required amount of electrical stimulation to the targeted location [64].

Closed-loop stimulation paradigms have been realized in some clinical applications, including neuromuscular stimulation in paraplegic subjects [2] and to control neural activity in epilepsy patients [17]. Closed-loop strategies have been used *in vivo* in animal models to control muscle excitations [18], to control the heart rate by electrical stimulation of the vagus nerve [63], and to modulate seizure activity [44], [47]. Closed-loop controllers have been used *in vitro* to adjust stimulation current to maintain the average firing rate at a desired inter-spike-interval [43], to correlate the spike timing between sets of arbitrary neurons [46], to control the firing rate of a neuron [43], to control the instantaneous response probability of a neuron [68], to control bursting dynamics in cortical cultures [67], and to identify different visual stimulus patterns that yield the same neuronal response [5].

Closed-loop control techniques to control neural activity have been investigated through simulation studies [24], [27], [55], [64]. Computer simulations of closed-loop techniques explored the possibilities to mimic the restoration of thalamocortical capabilities [24], to control simulated limbs movement [45], to adjust stimulation parameters to reduce simulated oscillatory neuronal activity [15], [55], and to control motion of a musculoskeletal system using a multilayer perceptron network feedforward controller combined with a feedback controller [49].

Various measures of the neuronal response can be taken into account for the closed-loop control and different performance measures can be incorporated. Closed-loop output measurements include ECoG signals [17], firing rate of individual neurons [68], spike timing of individual neurons [46], inter-spike-intervals [43], and electrical activity of population of neurons recorded with multi-electrode array [67]. Closed-loop performance measures included difference between target and average achieved median firing rate [67], percentage of decrease in seizure frequency [17], speed of correcting errors, and robustness of the system for different controller gains [43].

While feedback control plays a fundamental role in modern technological systems [23] and has many desirable properties including the capacity to improve robustness with respect to disturbances, to decrease sensitivity to model errors, and to stabilize an unstable system, its full advantages have not been utilized in medical bionic devices. In this study, we present a comparison of closed-loop and open-loop stimulation techniques to control neural activation in the retina. We investigate through simulation the advantages of using a closed-loop strategy; in particular, we demonstrate the

controller's robustness to disturbances and parameter uncertainties. Our motivation comes from retinal prostheses applications [69], [59].

We propose a model-based controller design for controlling activation of surviving neurons in people with retinitis pigmentosa (RP) and age-related macular degeneration (AMD). RP and AMD are examples of retinopathies that involve photoreceptor loss leading to eventual loss of vision. Postmortem analysis of the retinae of RP and AMD patients reveals that a large number of retinal neurons survive [36], [40], [41]. It has been shown that it is possible to elicit a sensation of light in RP and AMD patients by electrically stimulating the surviving neurons in the retina by means of visual prosthetic devices [4], [30]. Electrical stimulation of a small area of neuronal tissue in the vicinity of each electrode may create light perception, called a phosphene. To adjust the size and brightness of the phosphene, stimulation parameters are currently adjusted post-operatively, with associated potential difficulties due to limited time available with patients and clinical resources. When several electrodes are stimulated simultaneously, the phosphene size and brightness may change depending on the combination of active electrodes. Testing visual perception on the activation of all possible electrode combinations may take a significant amount of time, and becomes impractical as the number of electrodes increases. Challenges of adjusting stimulation parameters post-operatively include difficulties quantifying and measuring patient's perception, a large number of degrees of freedom, the complexity of the responses, and changes in neuronal responses over time.

The electrophysiology and topology of retinal neurons pose issues that are specific to this particular neural application. The first issue is a high density of RGCs compared to a low number of electrodes. A large difference between the density of electrodes and the density of neurons, in our case, leads to lack of controllability and observability of the whole system due to the fact that neurons are not interconnected. While control of individual neurons is not possible, to deal with a system that has a much smaller number of actuators and sensors (electrodes) than the number of systems states (neurons), we use Kalman decomposition to control a linear combination of neuron states of the system that correspond to a controllable and observable subspace in our model. We assume that the retinal ganglion cells (RGCs), the output neurons of the retina that transmit visual information to the brain, are not connected to each other. They act as outputs of communication buses that transmit information in parallel and do not exchange signals between each other. This known to not be the case because of gap junctions connecting the same ganglion cell types, but these are assumed not to play an important role and are neglected in the present analysis.

The main contribution of this paper can be summarized as follows. We propose the use of a model-based closed-loop design (a linear quadratic regulator in combination with a feedforward controller) to adjust stimulation parameters based on a linearized model of neural dynamics and a desired reference signal. To deal with the lack of controllability and observability of the whole system, we use Kalman decomposition and control only the controllable and observable part. Then, the dynamics of a linear combination of neurons (that represent the controllable and observable subspace of the system) can be controlled. In simulations, we are able to achieve acceptable performance despite a small number of actuators and sensors. We show that the closed-loop controller performs better than the open-loop controller when perturbations are introduced into the system. We envisage that our work will pro-

vide a better understanding of the opportunities and limitations of the closed-loop control, leading to more research and clinical investigations on the use of closed-loop techniques in bionic devices.

The paper is organized as follows. In Section 2, we derive a simple model suitable for the controller design and describe the feedback system set-up. In Section 3, we present the results of the simulations. Discussion and conclusions are given in Section 4.

2 Methods

A block-diagram of the open-loop system is illustrated in Figure 1, where K is the feedforward controller gain; its calculation is described below. For the purposes of this paper, the model of the neural response replaces the experimentally observable response of a neuron (illustrated in the figure by a cartoon of a neuron). x is the state of the system, y is the measured output, u is the controller signal. The controller signal is the electrical stimulation amplitude and the measured output is a measure of neural activity. The reference is neural activity of neurons in response to light stimulation, the controller is trying to adapt the stimulation level in order to replicate the response of neurons to light stimulation. Typically, the neural activity is quantified as the measured spiking rate of neurons. However, for simplification, in our case, we use the level of the neuron's membrane potential as an indication of neural activity of the neuron.

A block-diagram of the closed-loop system is given in Figure 2. In the diagram, $\bar{C}_r^*$ is the observer matrix, K_c and K_r are feedforward and feedback controller gains; their calculations are described below. The response of neurons to electrical stimulation is measured and used for controller design to calculate the electrical stimuli.

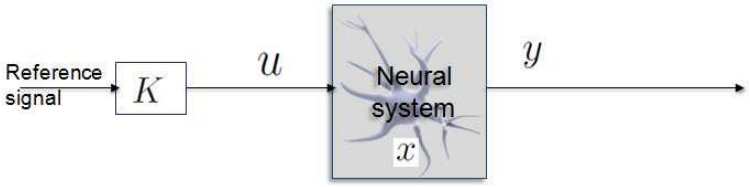

Figure 1: Open-loop system with a feedforward controller. K is the feedforward controller gains, u is the controller signal, y is the measured signal, x is the state of the system.

2.1 Geometry of the system

A schematic of an electrode array and neural tissue is given in Figure 3. An example array consists of 4 x 4 point electrodes that are separated equidistantly by 125 μm and a cell tissue area of 0.5 mm^2. In simulations, we also explored 8×8, 16×16, and 32×32 electrode arrays with a centre-to-centre pitch of 125 μm. The cell tissue area was scaled according to the size of the electrode array.

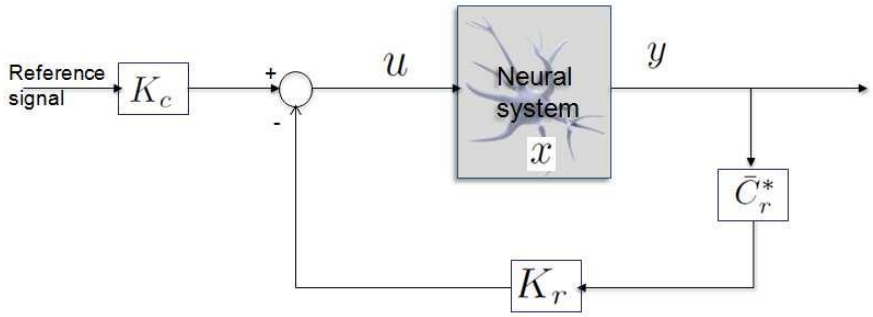

Figure 2: Closed-loop system with a static observer, feedforward and feedback controllers. $\bar{C}_r^*$ is a static observer matrix, K_c and K_r are feedforward and feedback controller gains, u is the controller signal, y is the measured signal, x is the state of the system.

In healthy human retina, the average density of RGCs depends on eccentricity, ranging from 2400 cells/mm^2 in the peripheral retina to more than 10^5 cells/mm^2 in the central retina [26]. To simplify the model, we use the cell density for peripheral retina. On average, 50% of RGCs survive in a retina of a person with AMD [41]. We assumed that the density of RGCs in degenerative retina is 1269 cells/mm^2, which corresponds to survival of 53% of RGCs. This corresponds to 317 cells in 0.5 mm^2 tissue; we round to 18 x 18 = 324 in order to have a rectangular grid of cells.

In the following, N is a number of neurons and M is the number of electrodes. The distance $H_{i,k}$ from each electrode $(i = 1, M)$ to each cell $(k = 1, N)$ is given in the matrix H,

$$H_{i,k} = (h^2 + |x_k - x_i|^2 + |y_k - y_i|^2)^{1/2}, \tag{1}$$

where (x_i, y_i, h) are the coordinates of the center of the electrode i, and $(x_k, y_k, 0)$ are the coordinates of the cell k, and h is the distance between the electrode array and the tissue. The distance $H_{i,k}$ from the highlighted electrode E_i to the cell S_k is illustrated in Figure 3.a.

The array is assumed to be $h = 60$ μm from the tissue, which is common for epiretinal visual prostheses.

2.2 Input into the system: retina response to light

Ideally, to use a static image or a video as a reference, the light intensity at each pixel of the image (each pixel of a video frame at each sampling time) has to be converted into a spike rate of a population of neurons in the topographic location corresponding to the pixel. To convert the light intensity into a neural population spike rate, a linear-nonlinear model can be used. A technique to estimate model parameters using white noise stimulus is given by Chichilnisky (2001) [9].

In this work, a static image or a video frame at each point in time is divided into N square pixels, where N is the number of simulated neurons. To convert the light intensity at each pixel into the membrane potential of neurons in the corresponding location, the light intensity at each pixel in the image is scaled from 1 to 256 with equal intensity increments between the steps. The light intensities are then used as

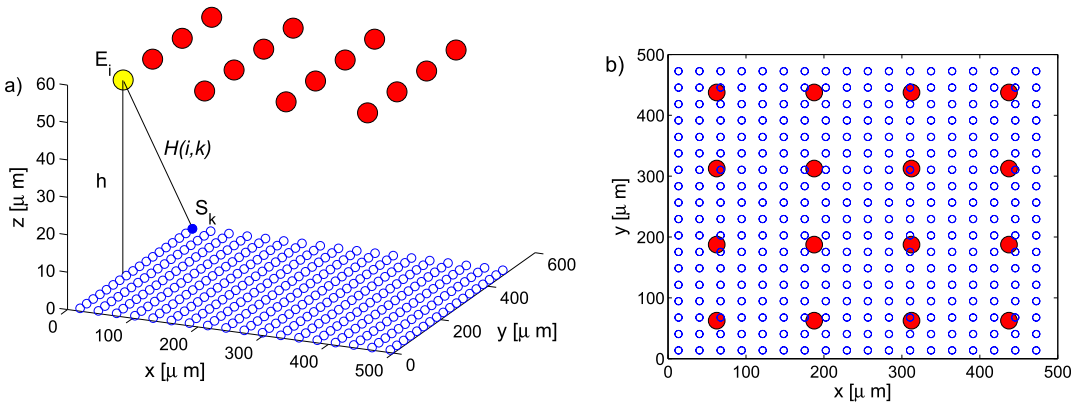

Figure 3: Geometry of the system. a) An array of 4 x 4 point electrodes at a distance $h = 60\mu$m above tissue. Tissue area is 0.5 mm^2. Distance between electrodes is 125 μm. Cell density is 1250 cells/mm^2. Red, yellow circle: electrodes; blue circles: cells. b) A birds-eye view of an array and tissue (z-axis is collapsed) with the same properties as in (a). Note, in this work, in all simulations and mathematical derivations, point source electrodes were used. Solid red and yellow circles are given for illustration purpose and do not correspond to the geometry of the electrodes used.

membrane potential references for the neurons in the corresponding locations. Note that these values do not correspond to the physiological values of the membrane potential.

2.3 Output of the system: retina response to electrical stimulation

In this section, we describe the model of the RGCs with sensor and actuator signals. The model of the RGCs was constructed from first principles based on modeling framework for electrical stimulation [42]. The models suitable for the controller design need to have some specific characteristics. The models need to be tractable and simple enough so that advanced control theory tools can be implemented and the calculation for the controller signal can be done on-line without requirement for high performance computational facilities. While there exist many models that describe neural response to sensory or electrical stimulation [9], [13], not all of them can be used for the controller design.

Often, to find a spike rate of a neuron, R_k, given its membrane potential, V_k, a sigmoid function is used [21]. A relationship between the spike rate and the membrane potential using a sigmoidal function is given in Figure 4. In this study, we assume that we operate in the region of the sigmoid that can be approximated by a linear function (red line), refer to the region between dashed lines Figure 4. This is a reasonable assumption, since the limit of RGCs response to electrical stimulation is 200 Hz, while the common stimulation frequency is 60 Hz (causing neurons to fire close to 60 Hz). Also, the range of the sigmoid that is to the left from this operating region, can be approximated by a zero spiking rate since many ganglion cells do not

exhibit spontaneous activity. Therefore, we assume that a neuron's spiking rate is proportional to the neuron's membrane potential and design a controller and observer for a linear neural response model. Note, it has been shown that linear models approximate well the individual ganglion cells response to electrical stimulation [32].

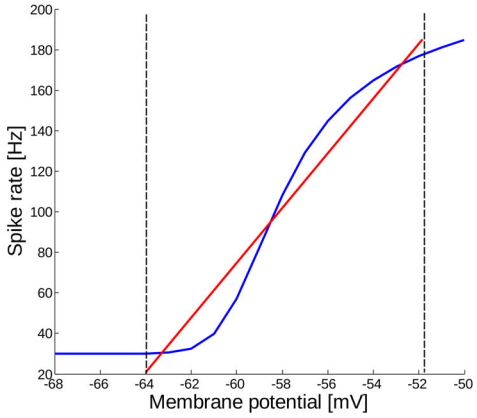

Figure 4: Blue: the relationship between the spike rate and the membrane potential using sigmoidal function. In the region between dashed lines, the sigmoid can be approximated by a linear function (red).

A common approach to investigate the fundamental mechanisms governing the effect of the extracellular stimuli on neuronal dynamics is based on the classical cable equation [52]. This approach can be extended to multiple compartments models [25] and different modes of stimulation in confined extracellular space [42]. We adopt the approach of modelling a neurite as a cylinder since it was shown that the ganglion cell's axon initial segment (represented here by a cylinder) shapes the cell's response to electrical stimulation [19]. Similar approach was used by Meffin et al. (2012) [42].

To model the effect of the electrical stimulation on the neural response, we derived a solution to the passive cable equation with current driving term for a point source stimulation electrode in a homogeneous medium. We calculate the transmembrane potential (hereafter, referred to as the membrane potential) due to a stimulating electrode at some distance from a neuron. The neurite is modeled by a homogeneous infinite cylinder driven by the local current density on a boundary of the cylinder. The extracellular space is confined and is modeled by a thin sheath with outer radius b surrounding the intracellular part of radius r_{a}; the intracellular and extracellular resistivities are equal, $\rho_{\mathrm{i}} = \rho_{\mathrm{e}}$. In the subthreshold regime the membrane behavior is linear and modeled by an RC circuit.

A common approach in the literature is to assume that the effect of the current passing across nerve fibre is negligible, [10], [52], [62]. Similar to these studies, we consider only the longitudinal mode of stimulation in which current passes into and along a nerve fibre oriented along the z-axis. In this case, the membrane potential, V, given the current density on a boundary of the cylinder, $J(z,t)$, is described by the cable equation:

$$\lambda_0^2 \frac{\partial^2 V(z,t)}{\partial z^2} - \tau_{\mathrm{m}} \frac{\partial V(z,t)}{\partial t} - V(z,t) = -\lambda_0^2 r_{\mathrm{e}} 2\pi\, bJ(z,t), \tag{2}$$

in which

$$\lambda_0^2 \triangleq \frac{r_\mathrm{m}}{r_\mathrm{e}+r_\mathrm{i}}, \qquad \tau_\mathrm{m} \triangleq r_\mathrm{m}c_\mathrm{m}, \tag{3}$$

r_i is the intracellular resistance per unit length, r_e is the extracellular resistance per unit length, $r_\mathrm{m} = R_\mathrm{m}/2\pi r_\mathrm{a}$ is the membrane unit length resistance, $c_\mathrm{m} = 2\pi r_\mathrm{a} C_\mathrm{m}$ is the membrane capacitance per unit length. r_a is the neurite radius, b is the radius of the extracellular space around the neurite. R_m is the membrane's unit area resistance, C_m is the membrane capacitance per unit area. The equation (2) in the frequency domain becomes:

$$\lambda^2(\omega)\frac{\partial^2 \hat{V}(z,\omega)}{\partial z^2} - \hat{V}(z,\omega) = -\lambda_0^2(\omega) r_\mathrm{e} 2\pi\, b\hat{J}(z,\omega), \tag{4}$$

where $\lambda^2(\omega)$ is the frequency dependent electrotonic length constant under current density boundary conditions,

$$\lambda^2(\omega) = \frac{\lambda_0^2}{1+j\omega\tau_\mathrm{m}}, \tag{5}$$

where j is the imaginary unit. Hats above variables denote Fourier transform in time.

We will use the following expression for the longitudinal component of the current density on the cylindrical boundary of the neurite due to a point source electrode in a homogeneous, isotropic medium. It can be derived from the expression for the current density due to a point source electrode ($I/4\pi R^2$) but finding the component on the normal current density on the cylinder boundary that is rotationally symmetric about the cylinder axis ([42],[61]) and using a Taylor expansion in b/H.

$$\hat{J}(z,t) = \frac{I(t)}{8\pi}\frac{b(2z^2-H^2)}{(H^2+z^2)^{5/2}}, \tag{6}$$

h is the distance between the electrode and the center of the neurite directly below the electrode, I is the applied stimulation current amplitude.

The Green's function which is the solution to equation (2) for $\hat{J}(z,\omega) = \delta(z)$ is found to be

$$\hat{V}^G(z,\omega) = \frac{r_\mathrm{e}\lambda(\omega)}{2} e^{-\frac{|z|}{\lambda(\omega)}}. \tag{7}$$

For any other current, the membrane voltage can be calculated through convolution integral in z

$$\hat{V}(z,\omega) = \hat{V}^G(z,\omega) * \hat{J}(z,\omega).$$

The maximal membrane potential occurs at $z = 0$. Inserting the expression (7) into (6) we obtain

$$\hat{V}(0,\omega) = \left[\frac{bZ_\mathrm{m}}{8\pi H^3} A((\lambda(\omega)/H)^2)\right]\hat{I}(\omega)$$

where Z_m is the specific membrane impedance, the part in the square brackets is the transfer function, and the function A is given by

$$A(x) = \int_0^\infty dz \frac{1-2xz^2}{(1+xz^2)^{5/2}} e^{-z}.$$

Using approximation an empirical observation that $A(x) = 1/(1+x)$, gives

$$\hat{V}(0,\omega) = \frac{b\hat{I}(\omega)}{8\pi H^3 C_{\mathrm{m}}(\tau^{-1} + j\omega)}$$

where $\tau = \left(\frac{1}{R_{\mathrm{m}}} + \frac{d}{\rho_{\mathrm{e}} H^2}\right)$, and $d = r_{\mathrm{e}} - b$.

From the above, we can calculate the effect of electrode i on cell k using the transfer function:

$$\hat{V}_k(\omega) = \frac{b\hat{I}_i}{8\pi H_{i,k}^3 C_{\mathrm{m}}(\tau^{-1} + j\omega)}, \tag{8}$$

where $\hat{V}_k$ is a Fourier time-transform of the membrane potential of the cell S_k, $\hat{I}_i$ is a current applied at the electrode i, and τ is the neural time constant for electrical stimulation, b is the width of the extracellular space surrounding a typical neuron, j is the imaginary unit.

In many applications, other neurons synaptically connected to neuron k also affect its membrane potential:

$$\hat{V}_k(\omega) = \frac{b\hat{I}_i}{8\pi H_{i,k}^3 C_{\mathrm{m}}(\tau^{-1} + \mathrm{j}\omega)} + \sum_l \hat{h}_{jl}(\omega)\hat{R}_l(\omega), \tag{9}$$

where $\hat{h}_{jl}(\omega)$ is the transfer function for the subthreshold response of the membrane potential for the synapse from neuron l to neuron k and $\hat{R}_l(\omega)$ is the Fourier transform of the spike rate of neuron l. However, for this application, we disregard network connections (input from other types of retinal neurons); i.e., the second term in the equation (9) is neglected since for many neuroprosthetic applications the injected electrical current has a much larger effect on the response of the neuron than the neuron's synaptic currents.

The influence of all electrodes on cell k can be calculated as

$$\hat{V}_k(\omega) = \frac{b}{8\pi C_{\mathrm{m}}(\tau^{-1} + j\omega)} \sum_{l=1}^{M} \frac{\hat{I}_l}{H_{l,k}^3}, \quad k = 1, \ldots, N, \tag{10}$$

where the effect of the combined stimuli are scaled by the inverse of the cubed distance between the electrode and the cell. According to (10), all electrodes have an effect on cell k. In reality, only electrodes in a limited vicinity, r_{e}, of the cell k have any appreciable influence onto its membrane potential; i.e.,

$$if \;\; (H_{l,k} > r_{\mathrm{e}}) \;\; \text{in} \;\; (10) \;\; \Rightarrow \;\; I_l \equiv 0. \tag{11}$$

r_{e} is varied in simulations (see Table 1).

Using the inverse Fourier transform of the right-hand side of (10), we can find how the membrane potential $V_k(t)$ changes over time,

$$V_k(t + \Delta t) = e^{-\tau^{-1}\Delta t} V_k(t) + \int_0^{\Delta t} e^{\tau^{-1}\Delta t\eta} \bar{B}_k d\eta \; u, \tag{12}$$

where

$$\bar{B}_k = \frac{b}{8\pi C_m} \sum_{l=1}^{n} \frac{1}{H_{l,k}^3}, \tag{13}$$

$k = 1, \ldots, N$.

Model parameters used in simulations are given in Table 1.

Table 1. Parameters of the model used in simulations.

Parameter	**Value**	**Description**	**Units**
D_{e}	cell density	1269	cells/mm^2
h	distance between the array and tissue	60	μm
r_{e}	radius of the influence of an electrode onto a neuron (varies in simulation)	[105,250]	μm
τ_{ref}	refractory time constant	5	ms
C_{m}	membrane capacitance constant	10^{-14}	$F\mu m^2$
τ	neural membrane time constant for electrical stimulation	1.1	ms
b	outer radius surrounding the intracellular part	0.5	μm

2.4 State-space representation

In this section, we rewrite the model in a state-space form that is more amenable to controller design. From (10), we obtain

$$\begin{cases} \dot{x} = Ax + Bu \\ y = Cx, \end{cases} \tag{14}$$

where $x \in \mathbb{R}^n$ is the state of the system, $y \in \mathbb{R}^m$ is the output of the system, and $u \in \mathbb{R}^m$ is the controller signal:

$$x := \begin{bmatrix} V_1 \\ \vdots \\ V_N \end{bmatrix}, \quad y := \begin{bmatrix} R_1^{\mathrm{av}} \\ \vdots \\ R_M^{\mathrm{av}} \end{bmatrix}, \quad u := \begin{bmatrix} I_1 \\ \vdots \\ I_M \end{bmatrix}, \tag{15}$$

where the controller action u describes the applied current on each electrode. In (14),

$$A = \begin{bmatrix} -\tau^{-1} & 0 & 0 \\ 0 & \ddots & 0 \\ 0 & 0 & -\tau^{-1} \end{bmatrix}, \quad B = \begin{bmatrix} \bar{B}_1 \\ \vdots \\ \bar{B}_N \end{bmatrix}, \tag{16}$$

A is a $N \times N$ matrix, τ is given in Table 1, $\bar{B}_k$ is given in (13), $k = 1, \ldots, N$, and

$$C = \begin{bmatrix} \frac{1}{H_{1,1}^3} & \cdots & \frac{1}{H_{1,M}^3} \\ \vdots & \ddots & \vdots \\ \frac{1}{H_{N,1}^3} & \cdots & \frac{1}{H_{N,M}^3} \end{bmatrix}. \tag{17}$$

2.5 Kalman decomposition

We found that the system (14) is neither controllable nor observable [23]. This is not surprising since we assume that the cells do not interact with each other and we have fewer electrodes than cells. However, as the matrix A is Hurwitz, the system (14) is detectable and stabilizable [23]. Hence, by stabilizing its controllable and observable part, we can stabilize the full system. We proceed by applying the Kalman canonical decomposition to (14). The Kalman decomposition decomposes (14) into parts that are observable and controllable (c, o), observable and not controllable $(o, \bar{c})$, not observable and controllable $(\bar{o}, c)$, and not observable and not controllable $(\bar{o}, \bar{c})$ [34]. We used MATLAB$^{\text{TM}}$ for all simulations.

Using Kalman decomposition, we transform (A, B, C) into $(\bar{A}, \bar{B}, \bar{C})$ using the following formulas:

$$\bar{A} = T^{-1}AT, \quad \bar{B} = T^{-1}B, \quad \bar{C} = CT \tag{18}$$

and use the new state of the system $z(t) = T^{-1}x(t)$, where T is $N \times N$ invertible matrix.

Matrices $\bar{A}$, $\bar{B}$ and $\bar{C}$ can be decomposed as follows:

$$\bar{A} = \left[\begin{array}{c|c} \bar{A}_{c,o} & \bar{A}_{\bar{c},o} \\ \hline \bar{A}_{c,\bar{o}} & \bar{A}_{\bar{c},\bar{o}} \end{array}\right], \quad \bar{B} = \left[\begin{array}{c} \bar{B}_{c,o} \\ \hline \bar{B}_{\bar{c},\bar{o}} \end{array}\right], \quad \bar{C} = \left[\begin{array}{c|c} \bar{C}_{c,o} & \bar{C}_{\bar{c},\bar{o}} \end{array}\right]. \tag{19}$$

Then, the full state-space representation of the transformed system is:

$$\begin{cases} \dot{z} = \bar{A}z + \bar{B}u \\ y_z = \bar{C}z, \end{cases} \tag{20}$$

where

$$z(t) = \begin{bmatrix} z_{c,o} \\ z_{c,\bar{o}} \\ z_{\bar{c},o} \\ z_{\bar{c},\bar{o}}. \end{bmatrix}.$$

During simulations, the upper right and lower left quadrants of $\bar{A}$, the lower quadrant of $\bar{B}$, and the right quadrant of $\bar{C}$ were close, but not equal, to zero due to numerical errors:

$$\bar{A} = \left[\begin{array}{c|c} \bar{A}_{c,o} & \cong 0 \\ \hline \cong 0 & \bar{A}_{\bar{c},\bar{o}} \end{array}\right], \quad \bar{B} = \left[\begin{array}{c} \bar{B}_{c,o} \\ \hline \cong 0 \end{array}\right], \quad \bar{C} = \left[\begin{array}{c|c} \bar{C}_{c,o} & \cong 0 \end{array}\right]. \tag{21}$$

Therefore, we consider only the observable and controllable part of the system (20). We use the variable $z_r = z_{c,o}$ to emphasize that the system we consider is a reduced-order system, where z_r corresponds to the observable and controllable part of the state in the Kalman decomposition form:

$$\begin{cases} \dot{z}_r = \bar{A}_r z_r + \bar{B}_r u \\ y_r = \bar{C}_r z_r, \end{cases}, \tag{22}$$

where

$$\bar{A}_r = \bar{A}_{c,o}\ , \ \bar{B}_r = \bar{B}_{c,o}\ , \ \bar{C}_r = \bar{C}_{c,o}, \tag{23}$$

and the applied stimulation current on electrodes is the controller action u.

2.6 Feedback controller design

In this section, we describe the feedback controller, provide a static observer design technique using the pseudo-inverse matrix, and characterize the signal used as a reference.

Linear quadratic regulator (LQR)

To control the observable and controllable part of the full system (20), a linear quadratic regulator (LQR) was implemented to control (22). The LQR is a well-known design technique that provides a feedback gain, K, in

$$u = -K_r z_r, \tag{24}$$

where

$$K_r = R^{-1}B^T P. \tag{25}$$

The technique is based on minimizing the quadratic cost function J in

$$J = \int_0^\infty (x^T Q x + u^T R u) dt, \tag{26}$$

where $R > 0$, $Q \geq 0$. This choice of cost function leads to algorithms that set the controller amplitude by minimizing the undesired deviations of the system's output from the reference signal. P is found by solving the continuous time Riccati equation,

$$A^T P + PA - PBR^{-1}B^T P = -Q. \tag{27}$$

The following R and Q that satisfy the conditions above were used in simulations:

$$R = \begin{bmatrix} r_1 & 0 & 0 \\ 0 & \ddots & 0 \\ 0 & 0 & r_M \end{bmatrix}, \quad Q = \begin{bmatrix} q_1 & 0 & 0 \\ 0 & \ddots & 0 \\ 0 & 0 & q_M \end{bmatrix}, \tag{28}$$

the values $r_i = 10$ and $q_i = 10^{-8}$, $i = 1, \ldots, M$, satisfied (26) and (27). These values are the design parameters; other values for R and Q can be used, which would lead to different controllers.

Feedforward controller in combination with LQR

A combination of feedback together with feedforward control can significantly improve the performance of the system over simple feedback control. A feedforward controller is especially useful when there are measurement disturbances in the system and there are modelling errors. Feedforward control can often reduce the effect of the measured disturbance on the system output much better than is achievable by feedback control alone. A feedforward controller with the gain K_c was added to the design:

$$K_c = \begin{bmatrix} k_{c_1} & 0 & 0 \\ 0 & \ddots & 0 \\ 0 & 0 & k_{c_1} \end{bmatrix}, \tag{29}$$

where the gain k_{c_1} is dependent on the number of electrodes and is given in Table 2. The values in Table 2 were obtained using simulations with different number of electrodes using optimization technique described in the Sub-Section 'Linear Quadratic Regulator'.

Table 2. Values of the feedback controller gain, k_{c_1}, vs the number of electrodes, M.

M	1	4	9	16	25	36	49	64	81	100	122	144	196	225	256
k_{c_1}	34.2	24	20.7	19.3	19.2	18.2	17.5	17.5	17.5	17.5	17.5	17.5	17.5	17.5	17.5

The resulting controller had the following form:

$$u = K_c r - K_r z_r, \tag{30}$$

where r is a reference. In the system (14), there are M inputs that correspond to the applied current amplitude at each of M electrodes. However, in the case when the reference is an image or a video frame, a number corresponding to each of N neurons is given, $N > M$. The reference has to be transformed from the dimension N into the dimension M. The old reference (r, corresponding to the state x) is transformed into the new reference (r_y, corresponding to the measurements y at each electrode) by $r_y = Cr$.

Observer design

In order to implement a static observer, only the observable and controllable part of the system (20) is considered, i.e. the system (22). The output of the system (22) has the following form:

$$y_r = \bar{C}_r z_r. \tag{31}$$

Since the matrix $\bar{C}_r$ is not a square matrix (the number of electrodes is not equal to the number of neurons), we use a pseudo inverse of $\bar{C}_r$ to calculate the static observer measurements,

$$z_r = \bar{C}_r^* y, \tag{32}$$

where the superscript * indicates the pseudo-inverse of the matrix.

Note, the system is partially controllable and the effect of the transformation in the Kalman decomposition is that the controller acts on the above variable $z-\mathrm{r}$ which is a linear combination of the original states, x, and the controllability of a neuron depends on its distance from the electrode (see definition of the matrix C in (17)).

2.7 Comparison of the closed-loop and open-loop stimulation strategies

In order to evaluate the advantages of using the feedback strategy to control activation of RGCs, we compare the performance of feedback and feedforward controllers when disturbances are introduced into the system.

We consider the system (14) with measurement noise h_{n} and parameter perturbations b_{n}, C_{n} in (16), (17). We design a controller for the reduced system with the

parameters given in Table 1: $h = 60$ μm, $b = 0.5$ μm, $C_{\mathrm{m}} = 10^{-14}$ F μm^2; however, we simulate the system with the parameters $h = h + h_{\mathrm{n}} = 70$ μm, $b = b + b_{\mathrm{n}} = 0.35$ μm, $C_{\mathrm{m}} = C_{\mathrm{m}} + C_{\mathrm{n}} = 10^{-13}$ Fμm^2.

The closed-loop controller was designed as given in Section 2.6. The open-loop controller for the reduced system (22) was designed as follows. Let the desired measurement be

$$z_r^* = \bar{C}_r^{-1} r, \tag{33}$$

where r is the reference signal. Let z_r^* be the equilibrium of the system (22). Then,

$$0 = \bar{A}_r z_r^* + \bar{B}_r u_r^*. \tag{34}$$

From (33) and (34), the open-loop controller is defined as

$$u_r^* = \bar{B}_r^{-1} \bar{A}_r z_r^* = \bar{B}_r^{-1} \bar{A}_r \bar{C}_r^{-1} r = Kr, \tag{35}$$

where $K = \bar{B}_r^{-1} \bar{A}_r \bar{C}_r^{-1}$ is the open-loop controller gain.

To replicate the current practice of manual tuning open-loop strategy in a lab environment based on the patient's perception, we manually tune the open-loop controller. We manually change the gain K in (35) while visually observing the output (the image). We set the gain K to the value that corresponds to the best possible image. Note, this manual tuning of the open-loop gain (and not the feedback gain) does not provide a fair comparison with the closed-loop controller. This "unfair" comparison is done specifically to show that even with this scheme, the closed-loop controller performs better than open-loop when disturbances are introduced into the system.

The evolution of the state and the output of the reduced system are compared using the closed-loop and open-loop stimulation strategies.

3 Results

3.1 Feedback controller

Extensive simulations to test the controller performance were carried out. The feedback system gave acceptable performance measured by the rate of convergence when a step reference is presented. For a unity step reference, the time of convergence was 0.12 s at which point the error was 0.1 mV. Note, the reference image was clearly recognizable much earlier than 0.12 s. In addition, the controller gains do not require on-line calculations (the gains are calculated off-line prior to dynamic simulations) and the controllers worked well with different numbers of electrodes.

To confirm that the state of the reduced system closely approximated the state of the original system, we compared the state and the output of the original system (14), the system in the Kalman decomposition form (20), and the reduced system (22). Note that the reduced system is the controllable and observable part of the system in the Kalman decomposition form. Refer to Methods for Kalman decomposition technique. The results plotted in Figure 5 illustrated that the original system (14), the system in the Kalman decomposition form (20), and the reduced system (22) respond in the same way. Simulations are done for 16 electrodes with 125 neurons; however,

only a subset of 3 references and 3 electrodes are shown for better visualization. Figure 5.a shows the recording electrode references for 16 electrodes; different colors represent different electrodes. The comparison of output of the systems is given in Figures 5.b, 5.c, 5.d. As observed in Figure 5, $y \cong y_z \cong y_r$, where y is the output of the original system (14), y_z is the output of the system in the Kalman decomposition form (20), and y_r is the output of the reduced system (22). In our case, the dimension of the outputs of the original system, the system in Kalman-decomposition form, and the reduced system are the same. Refer to the definition of the matrix $\bar{C}$ in (21) (the not controllable and not observable part of $\bar{C}$ is zero). Note, that the errors between the outputs of the original, the reduced, and the system in Kalman decomposition form were of the order 10^{-16} mV.

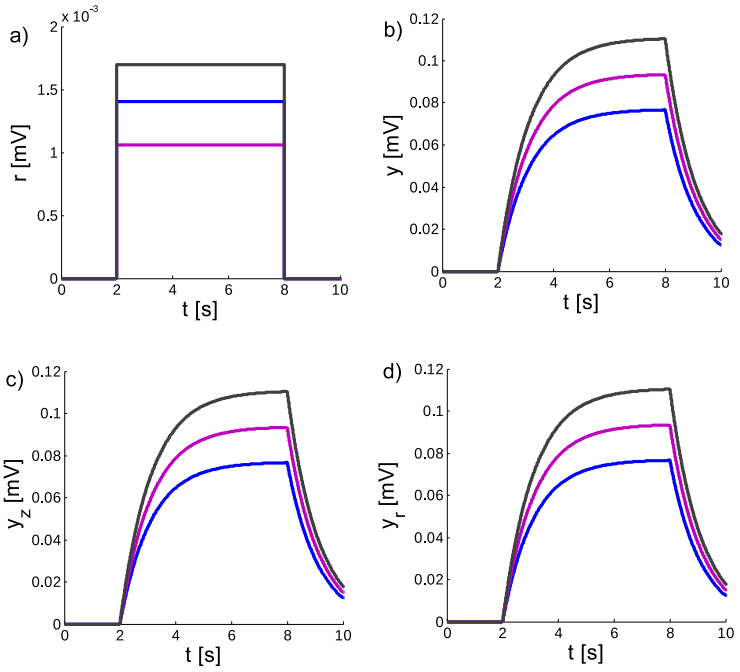

Figure 5: Comparison of the outputs (corresponding to 16 electrodes) of the original systems (14), the system in the Kalman decomposition form (20) and the reduced system (22). Simulations for 16 electrodes with 125 neurons. Only a subset of the 3 electrode references and corresponding 3 measured outputs is plotted for clarity. a) Recording electrode references for 3 electrodes. b) Output of the original system (14). c) Output of the system in the Kalman decomposition form (20). d) Output of the reduced system (22). Different colors represent different electrodes. The color of the trajectory in subplot (b) corresponds to the same color of the reference in subplot (a); similar for subplots (c) and (d).

The electrodes were chosen to produce distinct outputs (approximately on the diagonal in Figure 3b).

To confirm that the system in Kalman decomposition form behaves the same as the original system, we compared the states of these systems. The state evolutions of the original system and the system in the Kalman decomposition form are illustrated

in Figure 6. Simulations are done for 16 electrodes with 125 neurons. Only a subset of 3 neurons are shown for clarity; different color trajectories represent different neurons. Note that the error between the state of the original system and the system in the Kalman decomposition form (20) is negligibly small (of the order 10^{-10} mV). Therefore, we can conclude that the state of the system in the Kalman decomposition form (20) approximates the state of the original system well: $z \cong x$. Note, the dimension of the state of the reduced system is smaller than the dimension of the original system due to the fact that the reduced system is only the controllable and observable part of the system. Therefore, a comparison of the outputs only of these systems has been made (refer to Figure 5).

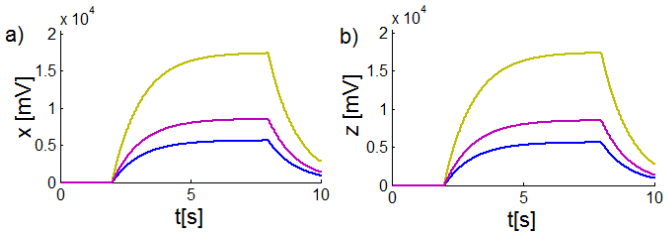

Figure 6: The state evolutions of the original system (14) and the system in the Kalman decomposition form (20). Simulations for 16 electrodes with 125 neurons. Only a subset of 3 neurons represented by three different colors is plotted for a better visualization. a) States of the original system, and b) States of the system in Kalman decomposition form. The errors between the states of the original system and the states of the system in Kalman decomposition form are of the order 10^{-15} when a step reference is presented.

Now we show that when using a controller designed for the reduced system we are able to track the reference signal with satisfactory performance. Simulation of the closed-loop system using 12 x 12 electrodes is shown in Figure 7. The figure shows that using the feedback controller, the reference to the system is approximated well. For these simulations, the image scrolls from right to left in 0.3 seconds; the subplot $a1$ shows a reference image. The subplot a2 shows an image of the state of the system converted into the light intensity at each pixel of the image. The analyzed area is represented by a red square in subplots a1 and a2. While simulations were done with 144 electrodes, only a subset of the references, states, and outputs of the system are illustrated for clarity. Figure 7.a shows relative values of the membrane potential corresponded to the image in a1 (that correspond to the intensity of light at each pixel). Figure 7.b shows the state of the original system. While the state of the system has some overshoot compared to the reference signal, the image a2 approximates the reference image a1 very closely. Figures 7.c shows the electrode references. Figure 7.d shows that the output of the system approximates the reference electrode signal with good accuracy. Different color traces in the figure correspond to different neurons and different electrodes, shown by solid circles in the subplots a1 and a2.

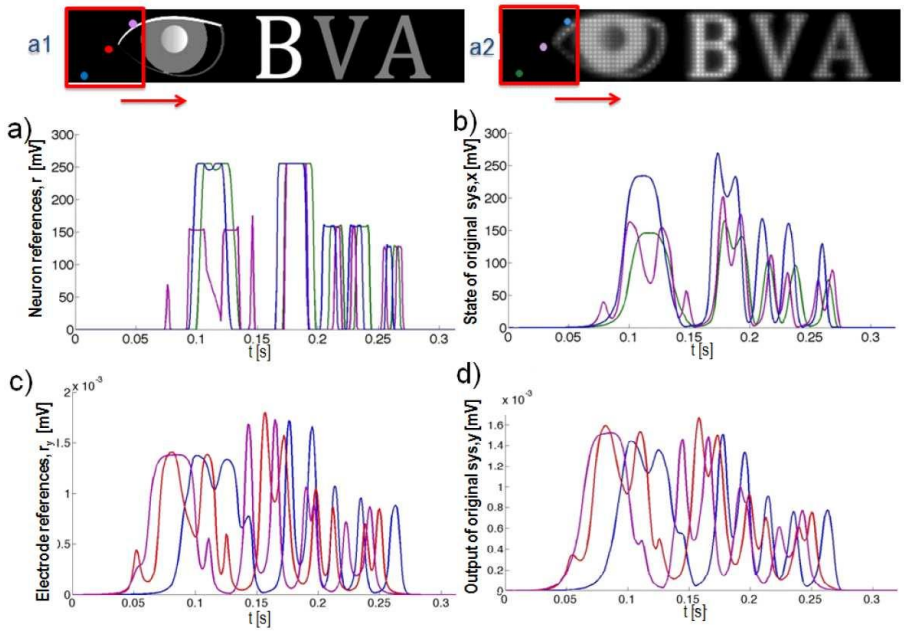

Figure 7: Simulation of the closed-loop system using 12 x 12 electrodes. The analyzed area is represented by a red square in the inserts a1 and a2. The image scrolls from left to right in 0.3s. (a1) Reference image and (a2) State of the system converted into the light intensity at each pixel of the image. The color of the trajectories in a,b corresponds to the same color neuron shown schematically in a2. The color of the trajectories in c,d correspond to the same color electrodes shown schematically in a1. a) Neuron references. b) State of the original system. c) Electrode references. d) Output of the original system. Only a subset of the electrode references and currents are illustrated for clarity.

3.2 Comparison of the closed-loop and open-loop stimulation strategies

A comparison of the closed-loop and open-loop stimulations strategies using 8 x 8 electrodes when there are no disturbances in the system is shown in Figure 8. The neuron references converted into light intensity at each point in the image is shown in Figure 8.a. Both stimulation strategies perform well and the reference is recognized using closed-loop stimulation (see Figure 8.b) or when the open-loop strategy is used (see Figure 8.c). This is not surprising since the open-loop controller can be tuned to track the reference signal with high accuracy when the model approximates the actual behavior of the system well. All simulations below are done for $r_{\mathrm{e}} = 125\mu$m.

However, the performance of the open-loop controller changes dramatically when disturbances are introduced into the system, as illustrated in Figure 9. While the closed-loop controller shows a robust performance (refer to Figure 9.b), the open-loop controller is shown to be highly sensitive to the system's uncertainties and measurement perturbations (see Figure 9.c). For these simulations, the controllers were designed for the reduced system with the parameters given in Table 1: $h = 60$ μm, $b = 0.5$ μm, $C_m = 10^{-14}$ F μm^2; however, simulations were run for the system with the parameters $h = h + h_{\mathrm{n}} = 70$ μm, $b = b + b_{\mathrm{n}} = 0.35$ μm, $C_{\mathrm{m}} = C_{\mathrm{m}} + C_{\mathrm{n}} = 10^{-13}$ Fμm^2 that corresponded to the measurement noise and parameter uncertainties. The

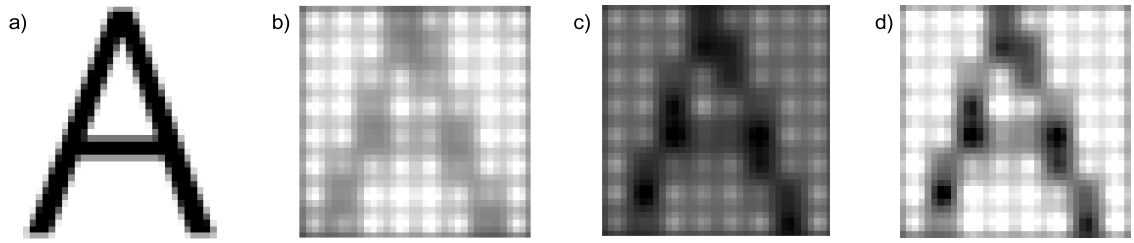

Figure 8: Comparison of the closed-loop and open-loop stimulation strategies using 8 x 8 electrodes with the system without disturbances. a) Neuron references converted into a light intensity at each point in the image. b) State of the original system using feedback stimulation strategy. c) State of the original system using feedforward stimulation strategy (35). d) State of the original system with manually adjusted feedforward controller gain.

neuron references converted into light intensity at each point in the image is shown in Figure 9.a. The reference, the letter "A", is recognizable when a closed-loop stimulation strategy is used even if significant disturbances are introduced into the system (refer to Figure 9.b; the online version has a better quality image). However, it is almost impossible to distinguish the letter when an open-loop controller is implemented (refer to Figures 9.d). This is a consequence of the open-loop gain calculation under the assumption of unknown disturbances. In reality, we can never estimate model parameters or disturbances perfectly. This result shows robustness of the feedback strategy with respect to the measurement disturbances and parameter uncertainties, and clearly indicates the advantages of using the feedback controller paradigm in comparison to the feedforward one. Note that the least controllable neurons lie on the perimeter of the image, since these neurons are not surrounded by electrodes. Due to that, there is a dark perimeter on the image using the closed-loop controller; these neurons do not receive substantial stimulation current to bring them to the higher activation state. Note that for simulations in Figure 9.b, a larger amplitude current was applied than in simulations for Figure 8.b. Therefore, the image in Figure 9.b is lighter.

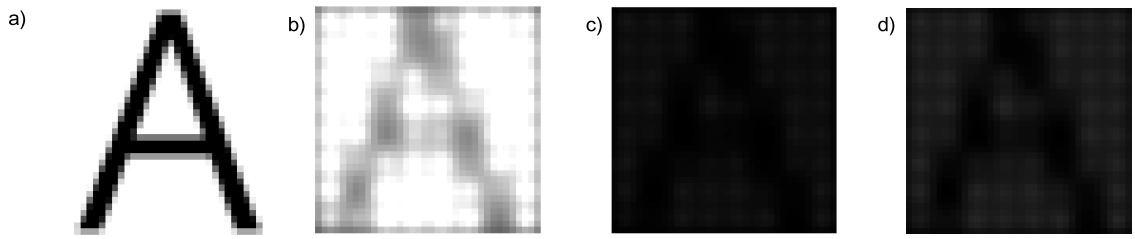

Figure 9: Comparison of the closed-loop and open-loop stimulation strategies using 8 x 8 electrodes for the system with disturbances. a) Neuron references converted into a light intensity at each point in the image. b) State of the original system using feedback stimulation strategy. c) State of the original system using feedforward stimulation strategy (35). d) State of the original system with manually adjusted feedforward controller gain set prior to introduction of disturbances.

4 Discussion and Conclusions

This paper provides a proof of principal of benefits for a closed-loop stimulation strategy to be used in a bionic device. This computational study is the first step towards potential clinical implementation of such stimulation paradigms. Benefits of computational models include relative ease of manipulations of the parameters of stimulation and making concrete predictions of the stimulation effect on the neural response.

We propose a simple linear model of neural activation for a model-based closed-loop controller design to adjust stimulation parameters dynamically based on the response of retinal neurons. Using Kalman-decomposition techniques, we are able to control linear combination of neurons and achieve acceptable performance. Our findings suggest that the closed-loop stimulation strategy offers some advantages over the open-loop strategy. We show that the closed-loop controller performs better than the open-loop controller when disturbances are introduced into the system.

A fundamental problem to convey sensory information using a bionic implant is to understand how electrical stimulation affects neurons. Biological systems are complex, and many approximations and simplifications are usually done in order to build a model of the neural response to electrical stimulation. The choice of the model used in this study is based on the fact that linear models are easier to analyze for the observability and stability criteria. It has been shown that linear models approximate well the individual ganglion cells response to electrical stimulation [32]. In addition, linear models offer a wider range of controllers that can be implemented. Note that in this work, we assumed that the neural activity can be described by the continuous intracellular membrane potential, whereas the measurements that are realistically accessible to a neuroprosthetic device are discrete spikes, from which the response strength can to be estimated by averaging over time or a population of neurons. This extension is left for future research.

Closed-loop strategy presented here compares more favorably to the open-loop strategy. Open-loop controllers can work well when the model of the system is known and the disturbances are measured. Often, an open-loop controller signal is found by inverting the model. In our case, however, due to model imperfections and unknown disturbances the open-loop controller performance is not satisfactory. On the other hand, the closed-loop controller shows robustness to model perturbations.

Closed-loop dynamic clamp is a standard procedure to measure ionic channel conductance [51], [58]. However there are many challenges to implement this method in clinical practice. While it is unlikely that many cells are controllable in a dynamic clamp individually, it is realistic that future prostheses can record neuronal activity extracellularly. However, this comes with many challenges including reliable on-line spike sorting and passing axons stimulations. A publications by Jepson et al. (2014a, 2014b) shows how retinal ganglion cells can be controlled individually using multi-electrode array stimulation [32], [33].

Feedback systems can be realized using standard *in-vitro* equipment. However, feedback strategies in neuroprosthetics have not been extensively investigated. A shift in paradigm to real-time closed-loop electrophysiology may provide many insights. With recent advancements in microelectronics, it may become feasible to test a range of closed-loop stimulation strategies in clinical settings in the near future.

The ability to continuously collect and analyze data may improve the monitoring of the disease progression and optimize the therapy efficacy. Novel sensing elements that measure electrochemical concentration may lead to stimulation paradigms that combine electrical stimulation with a drug delivery system.

A direct representation of neural activity as a gray scale image may not necessarily be the best approximation of the resulting perception of a patient. However, there is no clear measure of the subject's perception in simulations. The measure of algorithm's performance as a grey scale image quality was taken as an approximation.

In this work, step-wise constant presentations of the stimuli were considered. Real-life applications will involve dynamic stimuli that may cause time delay in the feedback system. Sufficient robustness conditions have to be derived under which the system remains stable, independent of the length of the delay. Some approaches for stabilization are introduced by Verriest et al. (1994) [65].

For safety reasons, short charge-balanced biphasic pulses are used in neuroprosthetic devices. In this paper, we implemented long monophasic pulse stimulation. We do not expect that this approximation will affect the results significantly. Future work include analyzing the response of neurons to different frequencies of stimulation, and investigating the effect of novel waveform shapes such as seesaw and sinusoids. In addition, maximum stimulation level, bandwidth limitations, the effects of the electrode geometry, and power requirements have to be investigated before implementing feedback controllers in clinical settings.

Acknowledgments

This research was supported by the Australian Research Council through the Discovery Early Career Researcher Award (DECRA) DE120102210. This research was supported by the Australian Research Council through its Special Research Initiative in Bionic Vision Science and Technology grant to Bionic Vision Australia. The Bionic Ear Institute acknowledges the support it receives from the Victorian Government through its Operational Infrastructure Support Program. NICTA is funded by the Australian Government as represented by the Department of Broadband, Communications and the Digital Economy and the Australian Research Council through the ICT Centre of Excellence program.

References

[1] Archbold S, Lutman ME, Nikolopoulos T. Categories of auditory performance: inter-user reliability. Br. J. Audiol., 32(1): 7 - 12, 1998.

[2] Abbas J.J., Chizeck H.J. Feedback control of coronal plane hip angle in paraplegic subjects using functional neuromuscular stimulation. IEEE Trans. Biomed. Eng., 38: 687 - 698, 1991.

[3] Aelen P., Aulanier A.L., Mintchev M.P. Feedback control of retrograde peristalsis using neutral gastric electrical stimulation. Proc. EMBS Conf., 3375 - 3380, 2008.

[4] Ahuja A.K., Dorn J.D., Caspi A., McMahon M.J., Dagnelie G., daCruz L., Stanga P., Humayun M.S., Greenberg R.J. Blind subjects implanted with the Argus II retinal prosthesis are able to improve performance in a spatial-motor task. Br. J. Ophthalmol., 95(4): 539 - 543, 2010.

[5] Bolinger D., Gollisch T. Closed-loop measurements of iso-response stimuli reveal dynamic nonlinear stimulus integration in the retina. Neuron, 73: 333 - 346, 2012

[6] Burkitt A.N. A review of the integrate-and-fire neuron model: I. Homogeneous synaptic input. Biolog. Cybern., 95: 1 - 19, 2006.

[7] Clark G. Cochlear implants: Fundamentals and Applications. Springer, 2003.

[8] Clark G. The multi-channel cochlear implant and the relief of severe-to-profound deafness. Cochlear Implants Intern., 13(2): 69 - 85, 2012.

[9] Chichilnisky E.J. A simple white noise analysis of neuronal light responses. J. Comput. Neural Syst., 12: 199-213, 2001.

[10] Coburn B. Neural modeling in electrical stimulation. Critical Reviews in Biomed. Eng., 17(2): 133 178, 1989.

[11] Colpan M.E., Ki Y., Dwyer J. et. al. Proportional feedback stimulation for seizure control in rats. J. Epilepsia, 48: 1594 - 1603, 2007.

[12] Cochlear implants: a practical guide. Edited by Cooper H.R., Craddock L.C. Wurr Publishers, 2006.

[13] Dayan P., Abbott L.F. Theoretical Neuroscience: Computational and Mathematical Modeling of Neural Systems. MIT Press, Cambridge, 2001.

[14] DiLorenzo D.J., Edell D.J., Kori M.J. et. al. Chronic intraneural electrical stimulation for prosthetic sensory feedback. Proc. EMBS Conf., 116 - 119, 2003.

[15] Feng X.J., Greenwald B., Rabitz H., Shea-Brown E.,Robert Kosu R. Toward closed-loop optimization of deep brain stimulation for Parkinsons disease: concepts and lessons from a computational model. J. Neural Eng., 4: L14-L21, 2007.

[16] Flora E.D., Perera C.L., Cameron A.L., Maddern G.J. Deep brain stimulation for essential tremor: a systematic review. Movement Disorders, 25(11): 1550 - 1559, 2010.

[17] Fountas K.N., Smith J.R., Murro A.M., Politsky J., Park Y.D., Jenkins P.D. Implantation of a closed-loop stimulation in the management of medically refractory focal epilepsy. Stereotact. Func. Neurosurg., 83: 153 - 158, 2005.

[18] Frankel M.A., Dowden B.R., Mathews V.J., Normann R.A., Clark G.A., Meek S.G. Multiple-input single-output closed-loop isometric force control using asynchronous intrafascicular multi-electrode stimulation. IEEE Trans. Neural Syst. Rehab. Eng., 19(3): 325 - 332, 2011.

[19] Fried S.I., Lasker A.C.W.,Desai N.J., Eddington D.K., Rizzo J.F.3rd. Axonal sodium-channel bands shape the response to electric stimulation in retinal ganglion cells. J. Neurophys., 101: 1972 - 1987, 2009.

[20] Freestone D.R., Aram P., Dewar M., Scerri K., Grayden D.B., Kadirkamanathan V. A data-driven framework for neural field modelling. Neuroimage, 56: 1043 - 1058, 2011.

[21] Gerstner W., Kistler W.M. Spiking neuron models: single neurons, populations, plasticity. Cambridge Univ. Press, 2002.

[22] Goffi-Gomez M.V., Abdala C.F., Peralta C.G.O. et. al. Neural response telemetry in patients with the double-array cochlear implant. Europ. Archiv. Otorhinolar., 267: 515 - 522, 2010.

[23] Goodwin G.C., Graebe S.F, Salgado M.E. Control system design. Prentice Hall, 2001.

[24] Gorzelic P., Schiff S.J., Sinha A. Model-based rational feedback controller design for closed-loop deep brain stimulation of Parkinson's disease. J. Neural Eng., 10, 2, 2013.

[25] Greenberg R.J., Velte T.J., Humayun M.S., Scarlatis G.N., de Juan Jr. E. A computational model of electrical stimulation of the retinal ganglion cell. IEEE Trans. Biomed. Eng., 46(5): 505 514, 1999.

[26] Harman A., Abrahams B., Moore S., Hoskins.R. Neuronal density in the human retinal ganglion cell layer from 16-77 years. The Anat. Record, 260: 124-131, 2000.

[27] Hauptmann C., Popovych O., Tass P.A. Effectively desynchronizing deep brain stimulation based on a coordinated delayed feedback stimulation via several sites: a computational study. J. Biol. Cybern, 93: 463 - 470, 2005.

[28] Hill B. Ionic channels of excitable membranes. Sinauer Associates Inc. Sunderland, Massachusetts, 1992.

[29] Hines M. NEURON a program for simulation of nerve equations. In Neural Systems: Analysis and Modeling, edited by F. Eckman. Norwell, MA: Kluwer, 1993.

[30] Humayun M.S., Weiland J.D., Fuji G.Y., et al. Visual perception in a blind subject with a chronic microelectronic retinal prosthesis. Vis. Res., 43(24): 2573 - 2581, 2003.

[31] Innes-Brown H., Marozeau J. M., Storey C. M., Blamey P. J. Tone, rhythm, and timbre perception in school-aged children using cochlear implants and hearing aids. J. Am. Acad. Audiol., (in press) 2013.

[32] Jepson L.H., Hottoway P., Mathieson K., Gunning D.E., Dabrowski W., Litke A.M., Chichilnisky E.J. Spatially patterned electrical stimulation to enhance resolution of retinal prostheses. J. Neurosci., 34(14): 4871 - 4881, 2014.

[33] Jepson L.H., Hottowy P., Weiner G.A., Dabrowski W., Litke A.M., Chichilnisky E.J. High-fidelity reproduction of spatiotemporal visual signals for retinal prosthesis. Neuron, 83: 87 - 92, 2014.

[34] Kailath T. Linear Systems. Prentice-Hall, 1980.

[35] Kalia S.K., Sankar T., Lozano A.M. Deep brain stimulation for Parkinson's disease and other movement disorders. Current Opinion, 26(4), 374 - 380, 2013.

[36] Kim S.Y., Sadda S., Pearlman J., Humayun M.S., de Juan E. Jr, Melia B.M., Green W.R. Morphometric analysis of the macula in eyes with disciform age-related macular degeneration. Retina, 22(4): 471 - 477, 2002.

[37] Klein D., Depireux D., Simon J., Shamma S. Spectro-temporal methods in primary auditory cortex. Publications of Center for Auditory and Acoustic Research. http://www.isr.umd.edu/CAAR/pubs.html.

[38] Lakhan S.E., Callaway E. Deep brain stimulation for obsessive-compulsive disorder and treatment-resistant depression: systematic review. BMC Research Notes, 3(60) 1 - 9, 2010.

[39] Lehmkuhle M.J., Bhangoo S.S., Kipke D.R. The electrocorticogram as a feedback control signal for deep brain stimulation of the subthalamic nucleus in the hemiparkinsonian rat. Proc. EMBS Conf., 1: 386 - 389, 2007.

[40] Margalit et. al. Retinal prosthesis for the blind. Surevy of Ophtalm., 47(4): 335 - 356, 2002.

[41] Medeiros N.F., Curcio. C.A. Preservation of ganglion cell layer neurons in age-related macular degeneration. Invest. Ophthalmol. Vis. Sci., 42: 795 - 803, 2001.

[42] Meffin H., Tahayori B., Grayden D.B., Burkitt A.N. Modeling extracellular electrical stimulation: I. Derivation and interpretation of neurite equations. J. Neural Eng., 9(6): 065005, 2012.

[43] Miranda-Dominguez O., Gonia J., Netoff T.I. Firing rate control of a neuron using a linear proportional-integral controller. J. Neural Eng., 7(6): 066004, 2010.

[44] Mogul D.J., Li Y., Colpan M.E. Using electrical stimulation and control feedback to modulate seizure activity in rat hippocampus. Proc. AES/ACNS conf., 46: 331, 2005

[45] Mohammed S., Poignet P., Fraisse P., Guiraud D. Toward lower limbs movement restoration with inputoutput feedback linearization and model predictive control through functional electrical stimulation. Control Eng. Practice, 20(2): 182 - 195, 2012.

[46] Muller J., Bakkum D.J., Hierlemann A. Sub-millisecond closed-loop feedback stimulation between arbitrary sets of indivisual neuron. Front. Neural Circuits, 6: 1-11, 2013.

[47] Nelson T.S., Suhr C.L., Freestone D.R., Lai A., Halliday A.J., McLean K.J. Closed-loop seizure control with very high frequency electrical stimulation at seizure onset in the GEARS model of absence epilepsy. J. Neural Syst., 21(2): 1-11, 2011.

[48] Niparko J.K. Cochlear Implants Principles and Practices. Lippincott Williams and Wilkins, 2009.

[49] Park H and Durand D.M. Motion control of musculoskeletal systems with redundancy. J. Biol. Cybern., 99(6): 503 - 516, 2008.

[50] Parker J., Karantonis D., Single P., Obradovic M. Compound action potentials recorded in the human spinal cord during neurostimulation for pain relief. Pain, 153(3): 593 - 601, 2012.

[51] Prinz A.A., Abbott L.F., Marder E. The dynamic clamp comes of age. Trends Neurosci., 27: 218 - 224, 2004.

[52] Rattay F. The basic mechanism for the electrical stimulation of the nervous system. Neurosci., 89(2): 335 346, 1999.

[53] Richard G., Keserue M., Hornig R. et.al. Long-term stability of stimulation thresholds obtained from a human patient with a prototype of an epiretinal retina prosthesis, Invest. Ophthalmol. Vis. Sci, E-Abstract 4580, 2009.

[54] Salam M.T., Sawan M., Nguen D.K. Implantable closed-loop epilepsy prosthesis: modeling, implementation and validation. ACM J. Emerg. Technol. Comput. Syst. 8(2), 1 - 18, 2012.

[55] Santaniello S., Fiengo G., Glielmo L., Grill W.M. Closed-loop control of deep brain stimulation: a simulation study. IEEE Trans. Neural Syst. Rehab. Eng., 19(1): 15 - 24, 2011.

[56] Schiff S.J. Neural Control Engineering: The Emerging Intersection between Control Theory and Neuroscience. MIT Press, 2011.

[57] Sinkjaer T., Haugland M., Inmann A. et. al. Biopotentials as command and feedback signals in functional electrical stimulation systems. J. Med. Eng. Phys., 25: 29 - 40, 2003.

[58] Sharp A., O'Neil M., Abbott L., Marder E., Dynamic clamp: computer-generated conductances in real neurons. J. Neurophysiol., 69: 992, 1993.

[59] Stingl K. et al. Artificial vision with wirelessly powered subretinal electronic implant alpha-IMS. Proc. R. Soc., 280: 20120077, 2013.

[60] Sykova E., Nicholson C. Diffusion in brain extracellular space. Physiol. Rev., 88(4): 1277 - 1340, 2008.

[61] Tahayori B., Meffin H., Dokos S., Burkitt A.N., Grayden D.B. Modeling extracellular electrical stimulation: II. Computational validation and numerical results. J. Neural Eng., 9(6): 065066, 2012.

[62] Tuckwell H.C. Introduction to Theoretical Neurobiology: Volume 1, Linear Cable Theory and Dendritic Cambridge Studies in Mathematical Biology. Cambridge Uni. Press, 1988.

[63] Tosato M., Yoshida K., Toft E., Nekrasas V., Struijk J.J. Closed-loop control of the heart rate by electrical stimulation of the vagus nerve. Med. Biol. Eng. Comput., 44: 161 - 169, 2006.

[64] Tukhlina N., Rosenblum M., Pikovsky A. et. al. Feedback suppression of neural synchrony by vanishing stimulation. J. Phys. Rev., 75: 01191.1 - 8, 2007.

[65] Verriest E.I., Ivanov A.F. Robust stability of systems with delayed feedback. Circuits Sys. Signal Proc., 13: 213 - 222, 1994.

[66] van Hateren J.H., Ruttiger L, Sun H., Lee B.B. Processing on natural temporal stimuli by macaque retinal ganglion cells. J. Neurosci, 15: 9945 - 9960, 2002.

[67] Wagenaar D.A., Madhaven R., Pine J., Potter S.M. Controlling bursting in cortical cultures with closed-loop multi-electrode stimulation. J. Neurosci., 25(3): 680 - 688, 2005.

[68] Wallach A. , Eytan D., Gal A., Zrenner C., Marom. S. Neuronal response clamp. Front. Neuroeng., 4: 1 - 10, 2011.

[69] Weiland J.D., Cho A.K., Humayun M.S. Retinal prostheses: current clinical results and future needs. Ophthalmol., 118: 2227 2237, 2011.